

## Results of Integrated Optimization of N=9 Quasi-isodynamic stellarator

V.D. Shafranov<sup>1</sup>, W.A. Cooper<sup>2</sup>, M.F. Heyn<sup>3</sup>, M.Yu. Isaev<sup>1</sup>, V.N. Kalyuzhnyj<sup>4</sup>, S.V. Kasilov<sup>4</sup>, W. Kernbichler<sup>3</sup>, M.I. Mikhailov<sup>1</sup>, V.V. Nemov<sup>4</sup>, C. Nührenberg<sup>5</sup>, J. Nührenberg<sup>5</sup>, M.A. Samitov<sup>1</sup>, A.A. Skovoroda<sup>1</sup>, A.A. Subbotin<sup>1</sup>, R. Zille<sup>5</sup>

<sup>1</sup> *Russian Research Centre "Kurchatov Institute", Moscow, Russia*

<sup>2</sup> *CRPP, Association Euratom-Confédération Suisse, EPFL, Lausanne, Switzerland*

<sup>3</sup> *Institut für Theoretische Physik, Technische Universität Graz, Graz, Austria*

<sup>4</sup> *IPP, NSC "Kharkov Institute of Physics and Technology", Kharkov, Ukraine*

<sup>5</sup> *Max-Planck-Institut für Plasmaphysik, IPP-EURATOM Association, Germany*

**Abstract** It has been demonstrated earlier that in quasi-isodynamic (qi) stellarators [1] with poloidally closed contours of the magnetic field strength on magnetic flux surfaces, good long-time collisionless confinement of  $\alpha$ -particles can be achieved simultaneously with stability of Mercier and resistive modes for different numbers of system periods (see, e.g. [2-4]). It was shown also that the effective-ripple factor  $\epsilon^{3/2}$ , which characterizes the neoclassical transport in the  $1/\nu$  regime, and the structural factor  $G_b$  of bootstrap current can be made small in configurations of this type.

It is of interest to find the configuration in which all the criteria of improvement could be satisfied simultaneously. In the present paper, preliminary results are presented of an integrated optimization of the  $N = 9$  qi configuration.

**Introduction** As was shown earlier, the quasi-isodynamic configurations with poloidally closed contours of  $B = \text{constant}$  on magnetic surfaces [1] possess such good properties as improved collisionless confinement of fast particle, small neoclassical transport and small bootstrap current. The value of the stability  $\beta$  limit in the configurations of such type depends on the number of periods and the aspect ratio. By numerical optimization, it was shown that a tendency exists of an increasing  $\beta$  limit with increasing number of periods [2-4]. In the present report, preliminary results of an integrated optimization toward quasi-isodynamicity (qi) are presented for a configuration with comparatively large number of periods,  $N = 9$ . Here the term "integrated" means that the penalty function is in particular weighting fast particle confinement, stability requirements and the requirement of  $\epsilon^{3/2}$  and  $G_b$  to be small.

**Results of the optimization** The optimization was carried out on the NEC SX-5 supercomputers himiko (Germany) and prometeo (Switzerland) with the VMEC code [5] for equilibrium calculations, the JMC code [6] for the transition to magnetic ( Boozer) coordinates and the MCT code [7] for the direct calculation of particle drift orbits. In addition, the global-mode stability of the optimized configurations was investigated with the CAS-3D code [8].

*Results of the initial optimization of particle confinement and local-mode stability*

The optimization was performed for a configuration with  $\langle \beta \rangle = 10\%$ . In the first step, the requirements of improved  $\alpha$ -particle confinement and local (Mercier, resistive-interchange and ballooning) mode stability was imposed. As a result, a configuration was found in which all collisionless  $\alpha$  particles born at  $1/2$  of the minor plasma radius were confined for a long time (there were no losses during the time of 1 sec considered for power-plant type parameters,  $B_0 = 5T, V = 1000m^3, \alpha$ -particle energy  $3.5MeV$ ). The stability investigation with the CAS-3D code has shown that the plasma is stable against

global modes up to  $\langle \beta \rangle = 14.5\%$ . In contrast to the previously considered  $N = 6$  configuration with  $\langle \beta \rangle = 5\%$ , a significant improvement of fast-particle confinement does not lead automatically to small effective ripple. The characteristic value of effective ripple was found to be  $\epsilon^{3/2} = 2 \cdot 10^{-2}$ . A possible cause is the large diamagnetic effect that occurs at high  $\beta$  that can lead to a correspondingly strong radial dependence of the poloidally averaged second adiabatic invariant  $\langle \mathcal{J} \rangle_\theta = \langle \oint V_{\parallel} dl \rangle_\theta$  so that the improvement of fast-particle confinement becomes possible even for a considerable poloidal variation of  $\mathcal{J}$ .

#### Results of the integrated optimization

To diminish the effective ripple and the bootstrap current, an additional optimization was performed with a corresponding target function. The  $\langle \beta \rangle$  value was chosen to be 11%.

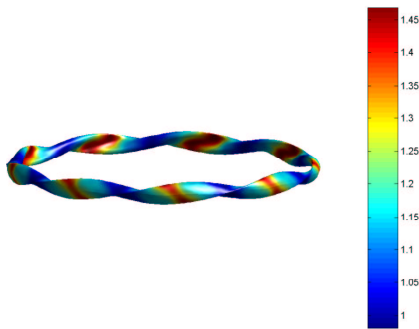


Fig. 1. Boundary magnetic surface of the optimized configuration also showing the magnetic topography. The colors define the range of the magnetic field strength.

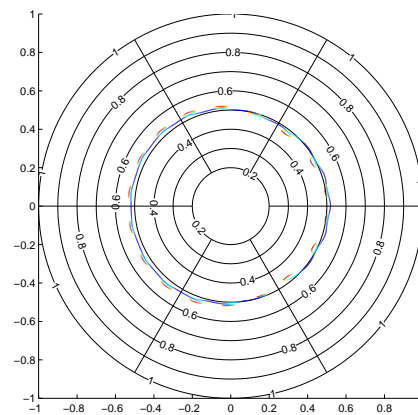


Fig. 2. Particle drift trajectory in the optimized qi configuration. The colors define the range of the particle parallel velocity (red – positive, blue – negative).

Fig. 1 shows the 3D view of the optimized configuration. The colors here define the magnetic field strength on the boundary magnetic surface. It is seen that the plasma column is almost straight in the regions of  $B$  extrema. Because of this structure of  $B$ , the reflected particles are trapped inside one plasma period, thus the banana size of trapped particles is quite small. Fig. 2 shows the projection of an  $\alpha$ -particle drift trajectory in coordinates  $(s, \theta_B)$ , where  $s$  is normalized toroidal flux and  $\theta_B$  is the poloidal Boozer coordinate. The colors here define the particle parallel velocity (red color corresponds to maximal (positive) value of  $V_{\parallel}$  and blue color corresponds to its minimal (negative) value). It is seen that on the outward part of the plasma column, a particle with positive  $V_{\parallel}$  is shifted to smaller plasma column minor radius while on the inward part the same parallel velocity leads to a particle shift outward. Thus, the bootstrap current in qi configurations appears adjustable to be nearly vanishing.

The behavior of the contours of  $B$  at 1/2 of the plasma minor radius is shown in Fig.3. Fig.4 shows the cross-sections of the plasma column at the beginning, at 1/4 and at 1/2 of a plasma period and the profiles of some flux functions.

The contours of the second adiabatic invariant, that describe the drift of banana centers, are shown in Fig. 5 for a set of particle pitch angles (i.e. for a set of values of  $B_{reflect}$ ). It is seen that these contours are well closed inside the plasma column for all pitch angles. As a consequence, the collisionless confinement of  $\alpha$ -particles is good. Fig. 6 shows the  $\alpha$ -particle collisionless losses in the optimized configuration as a

function of the time of flight. The particle orbits followed are initiated at 2/3 of plasma minor radius (there are no losses for particles born at 1/2 of the minor radius during the time considered). The calculations are performed for a power-plant type device.

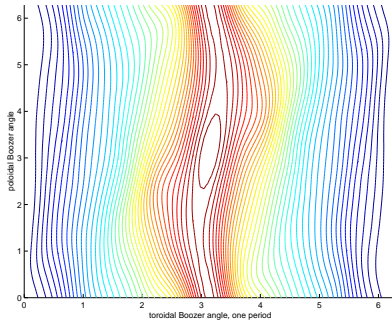


Fig. 3. Contours of  $B$  on the magnetic surface with  $s = 0.25$  for the optimized configuration.

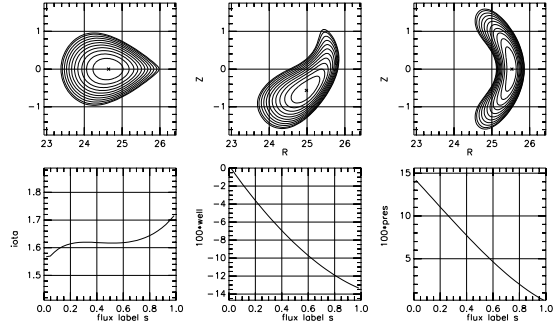


Fig. 4. Cross-sections of optimized configuration for  $\langle \beta \rangle = 11\%$ .

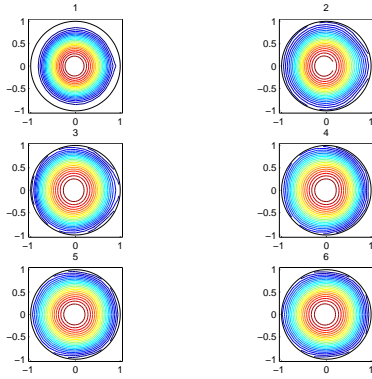


Fig. 5. Contours of the second adiabatic invariant in polar representation ( $\sqrt{s}$ , poloidal angle  $\theta_B$ , where  $s$  is normalized toroidal flux) for a set of increasing  $B_{reflect}$ ; 1 – corresponds to deeply trapped, 6 – to barely reflected orbits.

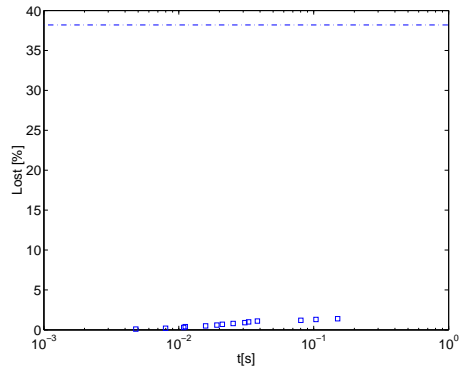


Fig. 6. Collisionless  $\alpha$ -particle confinement in the optimized configuration as a function of the time of flight. Particles are born at  $s_{start} = 0.44$  (2/3 of plasma minor radius), the dashed line shows the fraction of the reflected particles.

Fig. 7 shows the radial profile of the effective ripple in the optimized configuration. The radial dependence of the structural factor of the bootstrap current is shown in Fig.8.

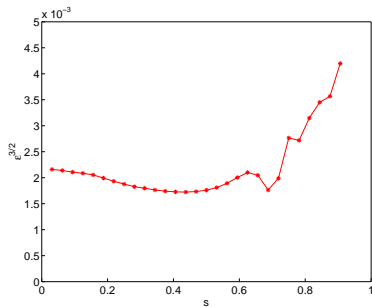


Fig. 7. Radial dependence of effective ripple for the optimized configuration.

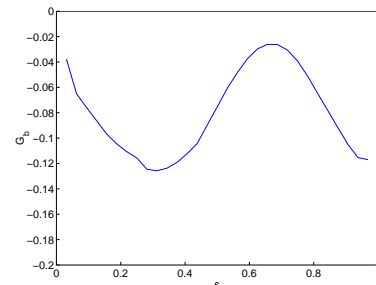


Fig. 8. Radial dependence of the bootstrap current structural factor for the optimized configuration.

The stability properties of Mercier and resistive-interchange modes are shown in Fig. 9. Fig. 10 shows the contours of the local-ballooning-mode eigenvalue as a function of the free parameters of the ballooning-mode equation,  $\theta_0, \zeta_0$ , for the magnetic surface with  $s = 0.6$ . Blue color corresponds to negative values (stable), red color corresponds to positive values. It is seen that two line-like regions of instability exist. The stability

